AIP Advances

A modified cryostat for photo-electrical characterization of porous materials in controlled atmosphere at very low gas dosage

Alessandro Cultrera, Giampiero Amato, Luca Boarino, and Carlo Lamberti

Citation: AIP Advances **4**, 087134 (2014); doi: 10.1063/1.4894074
View online: http://dx.doi.org/10.1063/1.4894074
View Table of Contents: http://scitation.aip.org/content/aip/journal/adva/4/8?ver=pdfcov
Published by the AIP Publishing

AIP ADVANCES **4**, 087134 (2014)

A modified cryostat for photo-electrical characterization of porous materials in controlled atmosphere at very low gas dosage

Alessandro Cultrera,[1,a] Giampiero Amato,[2] Luca Boarino,[2] and Carlo Lamberti[1,3]

[1]*Department of Chemistry, NIS Centre of Excellence and INSTM Reference Center, Via Quarello 11, Universit di Torino, 10135 Torino, Italy*

[2]*Electromagnetic Division, I.N.Ri.M., Strada delle Cacce 91, 10135 Torino, Italy*

[3]*Southern Federal University, Zorge street 5, 344090 Rostov-on-Don, Russia*

(Received 17 April 2014; accepted 9 August 2014; published online 25 August 2014)

We developed an integrated system for photo-electrical characterization of materials for sensing applications in strictly controlled environment conditions. The peculiar aspect of this setup is the capability of a fine-tuned gas dosage and a fast dynamic chamber pressure control, coupled with current and voltage sensing within a modified cryostat. To illustrate the capabilities of our system we have characterised both p^+-type mesoporous silicon (meso-PS) membranes and nano-crystalline mesoporous titanium dioxide (nc-TiO_2) films. In particular, as a main topic is presented a well-resolved characterization of mesoporous silicon electrical conductivity changes induced by presence of ethanol. At low pore filling level adsorbate-shunted conduction is avoided, while dielectric screening effects on frozen doping centres are observable. Beside we presented observation of mesoporous titanium dioxide photo-conductivity as a function of different gas pressure reporting opposite effects of relatively low- and high-pressure regimes. High reproducibility provided by the system is discussed as a final remark. [http://dx.doi.org/10.1063/1.4894074]

I. INTRODUCTION

Nanostructured semiconducting materials of large specific surface (100–500 m^2cm^{-3}) have been widely studied in recent years for several applications, one of them being sensing, with increasing the need for performing measurements in highly controlled ambient conditions[1–4] Dealing with such materials and systems, even small fluctuations in ambient conditions induce large variation in their response when the measurement precision is significant, making difficult a fine and reproducible characterisation. Since in some cases sensitivity of ppb level has been reported, a very accurate control of the experimental environment will be necessary in any future activity to approach lower and lower detection levels.[5,6]

Moreover, in this kind of materials, given the large surface to volume ratio, extrinsic phenomena like electronic transport through adsorbates easily overwhelm bulk effects. This is a strong limiting factor when investigating intrinsic properties of materials.

In order to be able to control such phenomena, we developed an integrated system for electrical characterization of materials for sensing applications in strictly controlled environment conditions modifying a commercial cryostat. To highlight the potentiality of this instrument, we investigated the reactivation of doping centers in mesoporous Silicon by dielectric screening of ethanol condensed within its pores. This is an example of bulk effect induced by the presence of a polar compound

[a]a.cultrera@inrim.it

condensed on the surface (but not completely filling the pores). In p^+-type meso-PS, free carriers due to B doping centers result frozen at room temperature, because of surface states trapping at low-coordinated silicon sites due to the peculiar subsurface position of Boron after the etching process.[7] These centers can be reactivated by the presence of a polar compound with large dielectric constant (e.g. ethanol $\epsilon_d = 25$). Under the action of its dielectric screening, the binding energy between trapped charge carriers and acceptor states in meso-PS will decrease resulting in increased free carrier concentration. A widely used technique for this kind of investigation is infra-red (IR) spectroscopy. IR spectroscopy measures changes in material absorbance (i.e. free carrier absorption), from which reactivation of frozen carriers can be evaluated, because absorbance is related to their actual concentration.[8–10] On the contrary electronic transport measurements could not in principle discriminate among the contributions of bulk free carriers and the conduction through adsorbed or condensed compounds. On the other hand, IR spectroscopy cannot discriminate among adsorption, condensation or pores saturation, or the transitions between them, while it is in principle possible by tracking electrical transport processes, provided that several parameters are finely controlled, as in our experimental setup. Additionally, the potentiality of the instrument is further evidenced by measuring the photoconductivity of nc-TiO_2 under different ambient conditions. We report for this task about the photoconductivity response in case of oxygen, nitrogen and dry-air dosages on samples that were previously left to equilibrate with certain background ambient conditions. TiO_2 revealed itself more sensitive to UV/Vis than our PS samples, hence more suitable for reporting about the illumination-related features of our system. TiO_2 is another widely investigated nanostructured material, with a band-gap of 3 eV.[11–13]

II. EXPERIMENTAL

A. System description

The system we implemented is based on a Janis ST-100 H cryostat equipped for fine-tuned gas injection driven by a Bronkhorst F201CV mass-flow controller (Ar calibrated), which can be connected to both a gas cylinder or a liquid container. The latter can be heated to achieve higher vapour pressures and to increase the stability of the mass-flow controller. F-201CV can reach a maximum flow of 10 sccm (see Figure 1 for a schematic description of the modified instrument). This model of cryostat was provided with four UV-grade fused silica optical windows. Two of them have been suppressed to gain a direct and independent access to the chamber for both gas injection and pumping (see Figure 1(a)), while the two remaining windows are available for any compatible optical purposes, even though, in principle, windows of different materials can be mounted, according to the wavelength of the employed radiation. The windows mounting position can be varied, in order to have them one in front each other, on opposite sides of the chamber, or sharing the same corner (angle of $\pi/2$) for optical applications in transmission or in reflection geometries, respectively. The system is additionally provided of a dry vacuum line to avoid back streaming of pollutant vapours from the pumps, a Varian SH-100 scroll pump and an Alcatel ATP 80 turbo-molecular pump. The pumping line is equipped with a manual Edwards Speedy-Valve™ just at the exhaust of the cryostat. This way the pumping efficiency can be also manually modulated in order to attain a wider pressure range. For measurements performed in vacuo, the system guarantees on the sample a vacuum down to $3.5 \cdot 10^{-5}$ mbar.

Both an E type thermocouple and a platinum Pt-100 resistive temperature sensor (DIN 43760 and IEC 751 Standard calibration down to 70 K) provide temperature sensing. An additional Pt-100 can be placed to perform temperature studies in remote mode (on the sample other than at the heater element). This additional sensor served also to test the temperature gradient between the sample holder and the electrical wiring late. A Lake-Shore 331 controller coupled with a liquid nitrogen transfer-line provides the sample holder temperature control and monitoring. The temperature controller features a standard P.I.D. feedback action. The temperature measurement precision was taken as 70 mK in the 77–550 K range. This depends on the electronic chain and the intrinsic limits of the sensor's calibration.

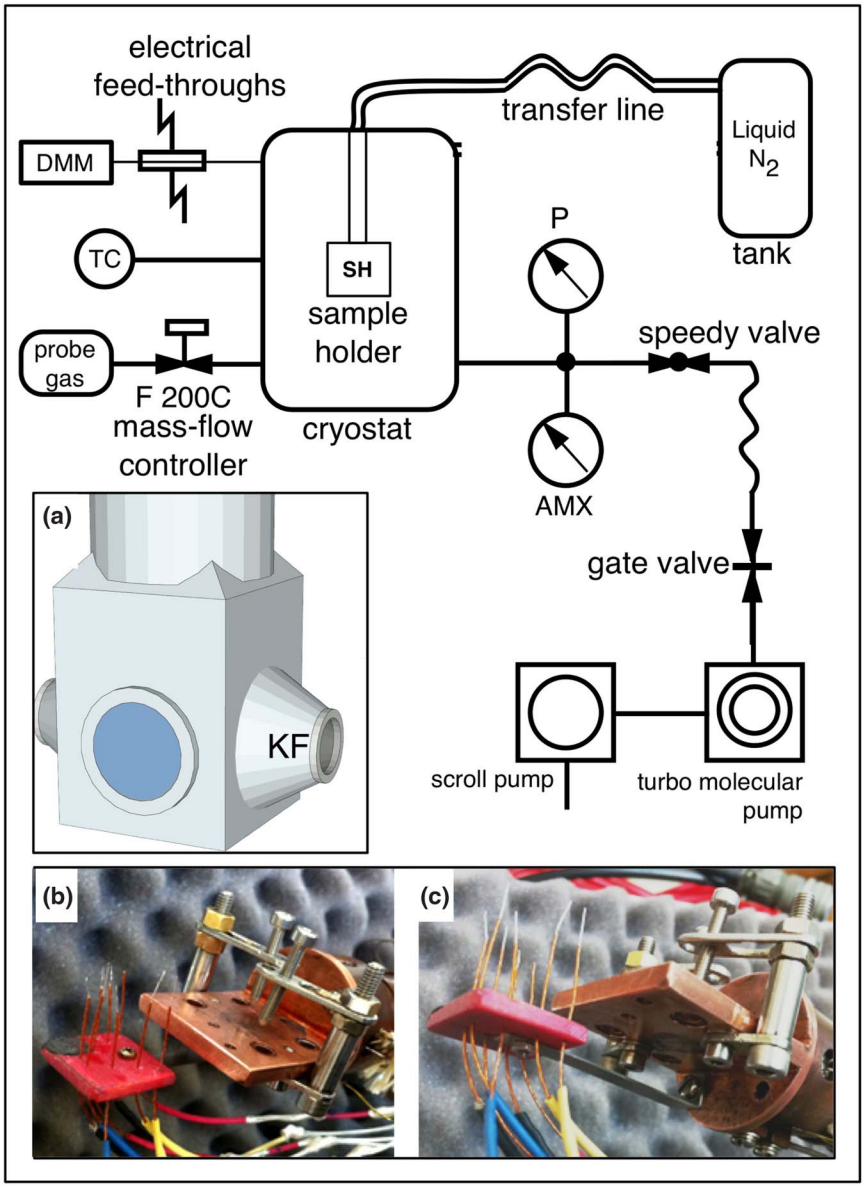

FIG. 1. Scheme of the experimental setup. The label "DMM" indicates the K2400 source-meter, "TC" the LakeShore 331 temperature controller, "probe gas" indicates a generic tank that can supply a probe gas through the mass-flow controller F200C. Labels "P" and "AMX" indicates the vacuum gauges. Inset (a) shows in detail the modified chamber of the cryostat with two of the optical windows substituted with KF-25 o-ring mounted connections (indicated by label "KF"). Inset (b) shows the top view of the modified sample holder ("SH" in the art line scheme). Inset (c) shows the detail of the electrical wiring plate mounted on a steel bar.

The sample holder at the end of the cold finger column has been modified to host a wider variety of samples. Two shafts with three degrees of freedom were added to the sample holder in order to mechanically fasten samples in the most suitable way. These end with screws provided of a teflon-covered tip. No blind screw-holes that could limit the pumping speed are present.

Instead of the original tip-probe system, the electrical wiring inside the chamber ends at the sample holder side with eight mechanically fastened pin connectors. Wires are AWG 42 gauge, 0.63 mm diameter, kapton sleeved were plug directly into a drilled fiberglass-polyester board (red plate in Figure 1(c)). This way there are no restrictions to the sample contact geometry, because the only request is the presence of two (or more) macroscopic pads on the sample support, while

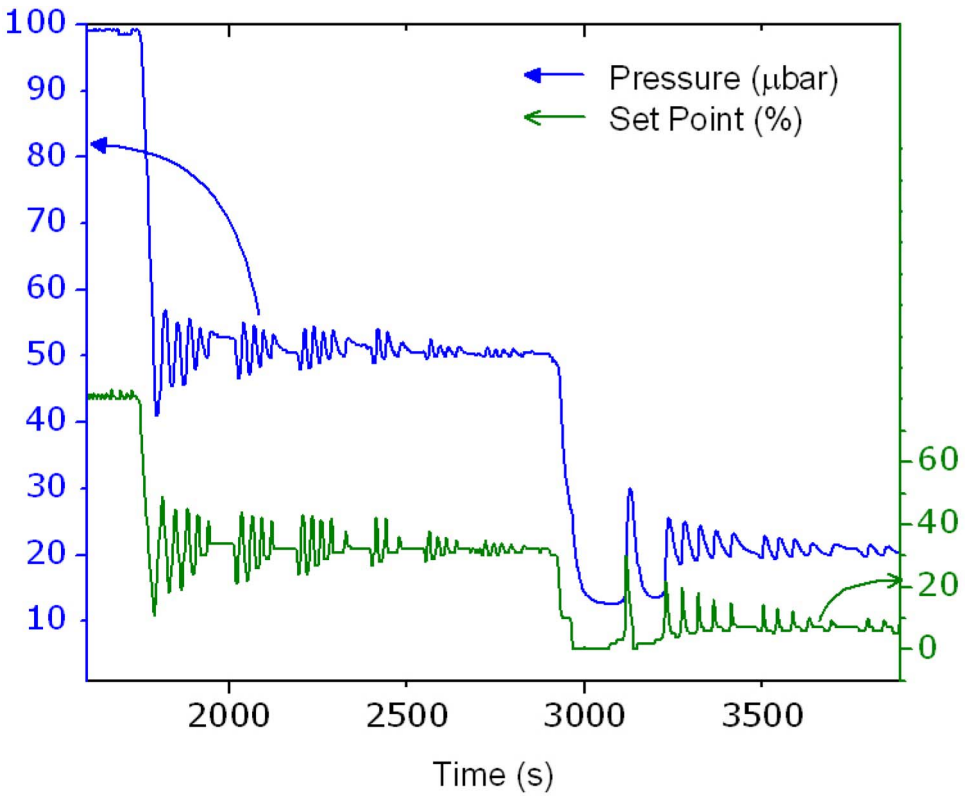

FIG. 2. Automated modulation of the mass-flow controller set-point (green curve, right ordinate axis) to reach new target pressures (blue curve, left ordinate axis). Starting from an initial equilibrium condition of 0.1 mbar of N_2, two successive pressure set points have been programmed, at 0.05 and 0.025 mbar.

the *in-situ* contact geometry can be engineered free of constraints, only depending on the sample itself.

The system is also provided with a Keithley 2400 SourceMeter™ for electrical measurements in different wiring configurations. Instead of the original tip-probe system, the electrical wiring inside the chamber (AWG 32 leads) ends at the sample holder side with a 8 pin male connector. This way there are no restrictions to the sample contact geometry, because the only request is the presence of two (or more) terminal pads for each sample on the support, and the on-sample contact geometry can be engineered free of constraints, only depending on the sample itself. Then it is possible to make connections between sample and measurement leads directly by means of small gauge gold wires. An ad hoc software interface has been realised within the LabVIEW™ environment. The flowmeter is driven by its own Flow-DDE™ server, which can be linked to LabVIEW by means of a proper library of subVis. The module devoted to reach and maintain a target pressure has a sampling rate of about 250 ms. The flow is controlled according to the target pressure by a feedback software module implemented within LabWIEW in which the readings from the vacuum gauges drive the mass-flow set-point. The solenoidal valve is driven by the Bronkhorst programmable proprietary P.I.D. feedback.

As an example of the ability of the system to react to successive requests of variation of the equilibrium pressure within the chamber is reported in Figure 2. Starting from an initial equilibrium condition of 0.1 mbar of N_2, the first target pressure was set to $5 \cdot 10^{-2}$ mbar. The target pressure is reached after 100 s, with oscillations of $\pm 1 \cdot 10^{-2}$ mbar. The amplitude of the latter is progressively dumped in time and after 400 s from the transient they are below $\pm 1.5 \cdot 10^{-3}$ mbar. Once the equilibrium has been reached, another step toward $2.5 \cdot 10^{-2}$ mbar follows, where the system reacts in a similar way. To reach and maintain the target pressure, the mass-flow controller set point automatically changes according with software parameters, see blue curve in Figure 2.

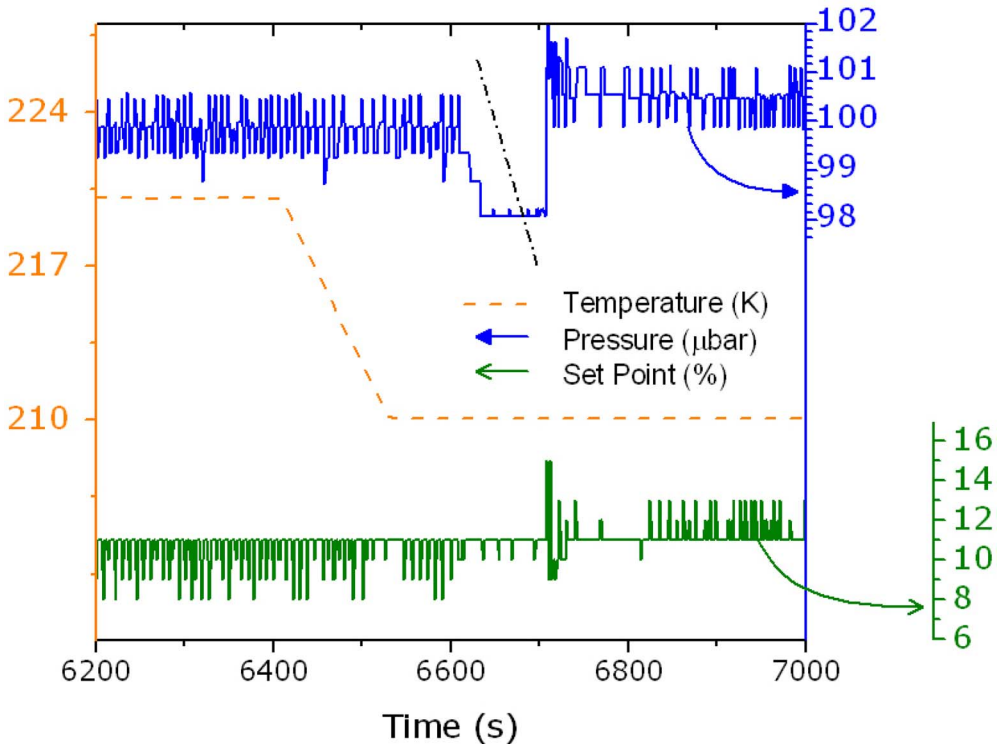

FIG. 3. Automated modulation of the mass-flow controller (set-point, black line, right black ordinate axis) to keep a constant pressure (blue line, right blue ordinate axis) over a programmed temperature change (red line, left ordinate axis). Dashed line-art indicates the starting drop in pressure due to condensation of ethanol for decreasing sample holder temperature.

Another example of the chamber conditions control is reported in Figure 3. The chamber pressure is 0.100 ± 0.05 mbar of ethanol at 220 K. As the temperature decreases to 210 K some ethanol condenses on the sample holder and the pressure tends to drop (see art-line in Figure 3 as a guide). To keep the constant target pressure the mass-flow controller varies the modulation and value of its set-point until a new equilibrium conditions is reached. As the temperature-induced pressure drop occurs (time = 6600 s) the feedback reacts and the target pressure is restored in about 100 s at the initial level within oscillations of ±0.05 mbar.

The software is designed to perform linear and logarithmic Current-Voltage or Current-Time measurements while simultaneously controlling temperature and pressure. The Keithley 2400, Lake Shore 331 communicate by standard GPIB 448.2 protocol, while a RS232 serial protocol drives the Edwards gauge controller.

A 6W UV tube lamp notch filtered at 365 nm have been used to expose titania thin films to band-gap light illumination. Light intensity on the sample was 20 μW cm^{-2}. Gases dosed during photoconductivity measurements on nc-TiO_2 was supplied from cylinders of laboratory grade gas (purity of ppb).

B. Sample preparation

Porous Silicon membranes have been prepared by electrochemical etching of p^+-type Si (Boron doped, resistivity 8–12 mΩ cm, ⟨100⟩ oriented). A teflon cell was filled with 25% HF aqueous etching solution (HF[50% in H_2O] 1:1 in ethanol) and several etching-rest cycles were performed (J = 325 mA cm^{-2} current density for 1 s and J = −0.1 mA cm^{-2} for 10 s). These membranes, 10 μm thick, were detached from the bulk silicon by a short electropolishing step at a current density of 1 A cm^{-2}, and moved on quartz plates. This kind of support prevents leakage current through the substrate during dc measurements. The porosity was calculated to be about 70% by gravimetric

measurements on sacrificial samples. Planar electrical contacts at a distance of 300 μm were made by means of a stencil mask with colloidal silver (Pelco 187).

Crosscheck measurements to test the effect of bulk ethanol as a shunt resistance have been performed on bulk silicon samples. These samples consisted in p-type silicon with 90 nm of thermal SiO_2 on the polished side. The conductivity of these oxide films is comparable to meso-PS, so it is possible to discriminate the effect of the sole ethanol in conductivity enhancement due to shunt resistance. Electrical contacts in planar configuration were painted with colloidal silver (Pelco 187) at a distance of 500 μm.

TiO_2 samples consisted in commercial electrodes for dye-sensitized solar cells (DSSC).[14] These were 15 μm thick mesoporous films of mostly anatase phase titanium dioxide deposed on conductive glass that served as bottom electrode (porosity around 60%). Measurements were conducted in stack geometry after the deposition of a graphite cement top electrode. For reproducibility considerations, similar anatase films, but with gold contacts in planar configuration, were used. These were obtained by screen printing of commercial anatase colloidal dispersion (Solaronix), and were 3.5 μm thick. The planar contact geometry allowed to host three samples per support (bare quartz). Detailed description of measurement preparation protocol for this reactive material are reported elsewhere.[15]

III. RESULTS AND DISCUSSION

This experimental set-up guarantees a fine control on the chamber pressure, better than 1% in the range of 10^{-2} mbar and even better at higher pressures. As already discussed in the experimental (Section II, Figure 3) by acting on the temperature of the sample holder it is possible to reach the gradual condensation of ethanol on the sample while maintaining a constant pressure in the chamber. Ethanol, in meso-PS experiments, was chosen for several reasons. We already performed spectroscopic studies on the same topic with ethanol filled meso-PS[10] and ethanol has one of the largest dielectric constants among polar solvents ($\epsilon_d = 25$). Moreover its condensation in the pores significantly increases the effective dielectric constant ϵ_{eff} of mesoporous Silicon membranes. Finally its freezing point at pressures of 0.1 mbar is at temperatures low enough (160 K) to achieve condensation and even pore filling, but no solid transition, within a broad temperature range. Another intriguing aspect is the possibility to verify that liquid-solid transitions for confined liquids is down-shifted.[16] In order to get rid of injection- or ionization-related effects, dc measurements on both meso-PS and TiO_2 samples were carried out at small applied voltages (electric field smaller than 10^2 V cm^{-1} in the present sample configurations).

A. Dielectric screening in meso-PS

In Figure 4 are reported two Arrhenius type plots. Diamonds represent the temperature dependence of conductivity for a porous silicon sample in vacuum after a thermal annealing (450 K for 30 min, 1 K min^{-1}) to clean the surface from adsorbed water from ambient. In meso porous silicon the electrical transport can be considered to be thermally activated as in standard semiconductors, because the crystalline structure is large enough (10–20 nm) to prevent quantum confinement effects.[17,18] A typical Arrhenius behavior is expected in absence of adsorbates.

Circles represent the characteristic for the same sample, at a pressure of 0.1 mbar of ethanol. Three main features are present. The first consist in a steeper decrease of conductivity for exposed meso-PS at high temperature (see Figure 4 inset). This can be related to the effect of donor-like surface states induced by adsorbed ethanol molecules.[9,19] Following this hypothesis, in this temperature range, the amount of ethanol adsorbed in the channels of the meso-PS is not enough to induce an effective dielectric screening within the bulk skeleton of meso-PS. The dominant effect is the formation of more donor-like states at surface that compensates the holes concentration.

The second feature is a jump (labeled "j" in Fig. 4 of the exposed curve, at about 210 K. The conductivity of the ethanol-exposed meso-PS sample crossing this temperature is $3.4 \cdot 10^{-13}$ S cm^{-1}, while in absence of ethanol it was $7.4 \cdot 10^{-14}$ S cm^{-1}. We assign to this feature the doping centers reactivation by dielectric screening of ethanol. In Eq. (1) is reported the expression for thermal activated electrical conductivity the pre-exponential factor σ_0 depends on free carrier concentration

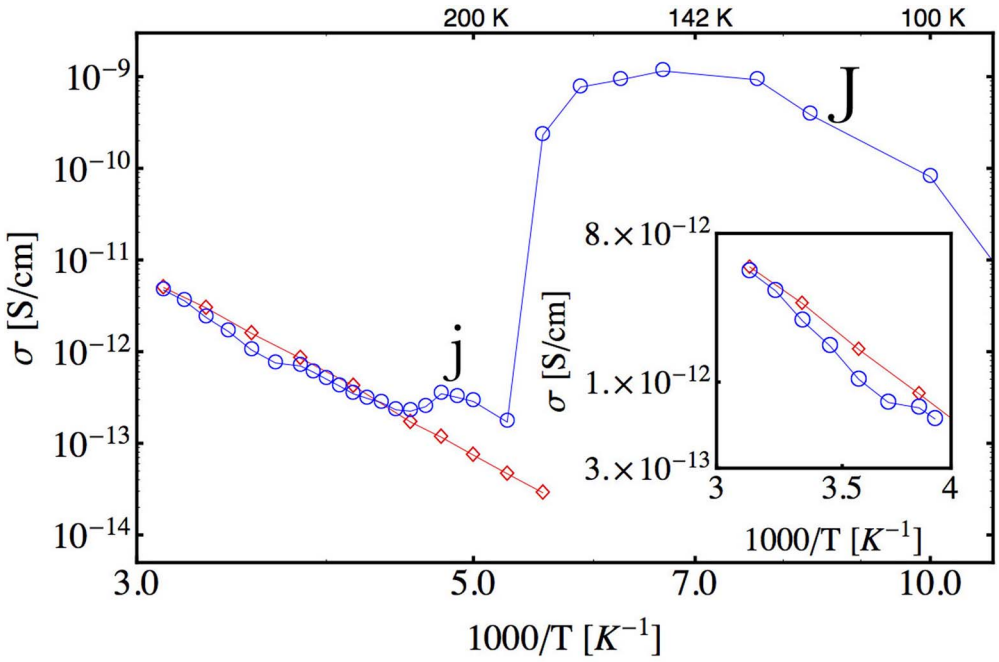

FIG. 4. Arrhenius plot of conductivity for bare (diamonds) and ethanol exposed (circles) PS at constant pressure of 0.1 mbar of ethanol vapour. The inset shows the detail around 320 K–280 K. The ethanol-exposed curve features two significant jumps labeled "j" and "J", as we refer to these in the text.

(p) and mobility (μ):

$$\sigma(T, p, \mu) = \sigma_0(p, \mu)e^{-(E_a/kT)}. \quad (1)$$

Note that the slope of the exposed sample curve in Figure 4 at 200–180 K exhibits a slope very similar to the unexposed one (and to itself before the first jump ("j"), indicating that only the pre-exponential factor of conductivity was significantly affected by ethanol. Hence the transport mechanism can be considered unchanged. FTIR measurements published elsewhere[10] showed a carrier reactivation due to ethanol dielectric screening on similar samples, but electrical transport measurements could also in principle account for mobility effects due to reduced coulomb blockade within transport paths.[20]

The third interesting feature is the huge jump (labeled "J" in Fig. 4 at 180 K of the exposed curve. We attribute this effect to the saturation of ethanol within the pores with a consequent shunting of the meso-PS porous network.

To justify our assignments, we made some calculations based on a Bruggerman effective medium approximation.[21] Under this effective medium approximation, for a porosity of 70%, the d.c. conductivity of ethanol-saturated meso-PS at RT would be about $1.4 \cdot 10^{-6}$ S cm^{-1}, against a common reported value for bare meso-PS conductivity[22] of about 10^{-10} S cm^{-1}. This means a difference of 4 orders of magnitude between unfilled and saturated meso-PS. Since in the present case the experimental conductivity of the exposed sample at 210 K is only a factor of 4.5 larger than the conductivity of the unexposed one, while at lower temperature occurs a huge jump, a complete saturation of pores at 210-180 K could be excluded and the enhancement is assigned to additional free carriers. Note that the reported conductivity at RT for ethanol in literature is lower than the value we used here for calculations.[23] We measured the conductivity of ethanol employed in this experiment in a two-electrode cell. However, a possible conductivity enhancement due to the typical impurities and moisture contamination of laboratory grade ethanol cannot be excluded. The situation is rather different for the third reported transition ("J"), around 180 K. Here the conductivity of the unexposed meso-PS $2.8 \cdot 10^{-14}$ S cm^{-1} while the exposed one it is $2.4 \cdot 10^{-10}$ S cm^{-1}, with indeed a 4 orders of magnitudes increment.

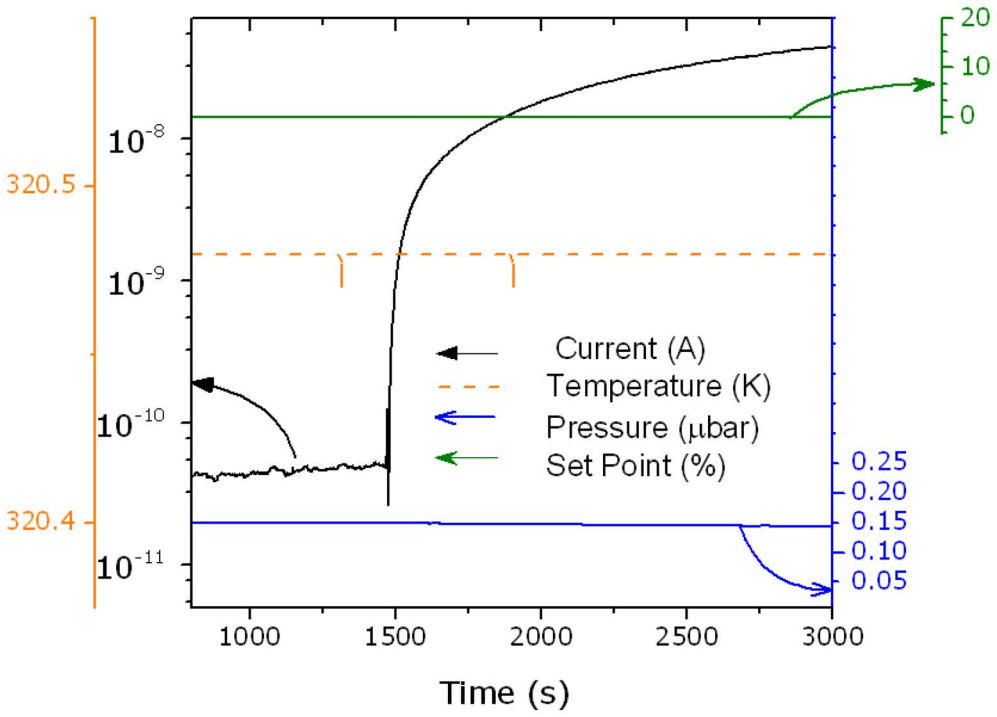

FIG. 5. TiO_2 photo-conductivity transient (black) after switching on UV light at 1500 s. To testify the stability of the system also the temperature of the sample (orange line), the pressure inside the cell (blue line) and the set-point (green line) have been reported.

As already pointed out, some confinement effects could be highlighted. Note that even at temperature lower than 160 K there is not an abrupt change in conductivity for exposed meso-PS. This suggests, in our opinion, that ethanol is not yet frozen on the surface nor within the pores os meso-PS.

The undershoots in σ(T) at 220 K and 180 K are due to the time for current to reach equilibrium at the beginning of the jumps of characteristics. We decided to set a maximum settling time of 1000 s for each point acquired to avoid excessive exposure to ethanol condensing vapour.

A crosscheck test performed on a bare Silicon oxide sample, confirmed that at low temperature, when exposed to ethanol vapour, the conductivity suffers an abrupt change with a jump of 3 orders of magnitude. This should confirm the nature of the third reported transition (Fig. 4 - "J"), and allowed us to assign the second (Fig. 4 - "j") one to dielectric screening effects on frozen doping centers.

B. Mesoporous TiO_2 photoconductivity under gas dosage and effects of background ambient

We performed experiments on mesoporous TiO_2 films in dark, for pressures below 5 mbar of dry-air (1 mbar O_2), and those did not highlight any substantial effect on the conductivity, while at 10^3 mbar the electron-scavenger nature of adsorbed oxygen have been observed clearly.

Concerning the experiments under illumination the effect of small gas dosages was instead remarkable. Under the reported illumination conditions, conductivity rose of about 5 orders of magnitude compared to dark conductivity at the same bias voltage (0.5 V), with extremely slow transients, reported in Figure 5 to reach equilibrium. This behaviour is consistent with other works on similar topics.[24,25]

Figure 6 reports the perturbation induced by pressure steps under constant illumination. In region "a" the pressure is kept constant at a minimum average value of $1.5 \cdot 10^{-2}$ mbar and the current is slowly decreasing after a preview run of the experiment. For our purposes it is not a

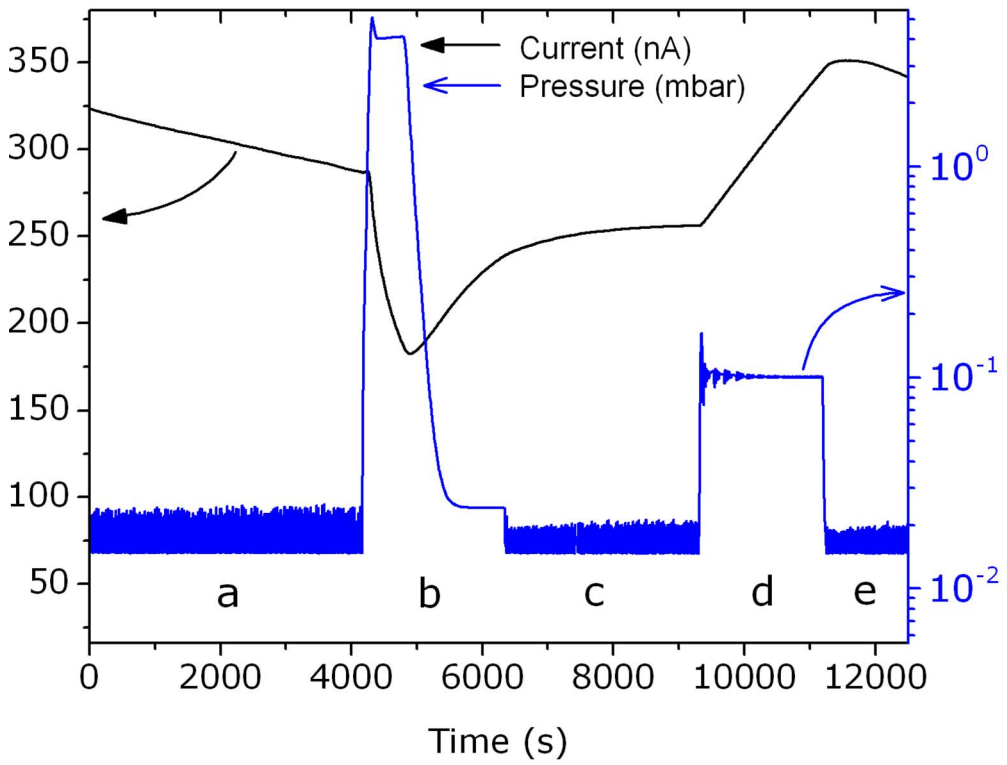

FIG. 6. Photoconductivity response of mesoporous TiO_2 under constant illumination (black line, left axis). Sample is biased at 0.1 V and exposed to 20 μW cm^{-2} of UV light at 365 nm. For higher dry-air pressure the conduction is quenched (region "b"), while at lower pressure the effect is opposite (region "d").

concern this not completely steady current. In region "b", at a pressure of 4 mbar of dry-air, the conductivity is degraded with a steep slope decay characteristic. The duration of the exposition to dry-air have been limited in order to limit the recovery time (region "c").

Conversely at lower dry-air pressure levels (region "d") the conductivity is enhanced. The last region "e" of the plot shows the slow relaxation transient after the small dosage and is consistent with region "a", in fact the initial current decrease (T < 4000 s) is the result of a preview small dosage like the one of region "d" as the sequence have been repeated during each run of the experiment. In the case of small dosage the exposition time was longer to attain a clear enhancement of photoconductivity because this effect is weaker than the one due to higher dry-air pressure.

Some considerations are necessary at this point. At any degree of vacuum achievable from the presented system, the TiO_2 films at a point reach equilibrium with the background chamber ambient. Background ambient, in absence of other sources (dosages from the mass-flow controller), is due to chamber leaks and pumps back-stream, roughly composed by N_2, O_2 and water similarly to the external ambient. So on the surface of TiO_2 a certain amount of adsorbed oxygen ($O_{2(ads)}$) and hydroxyl groups (OH) are always present and affect concentration and mobility of excess photo-electrons. In particular electron trapping at $O_{2(ads)}$ sites (Eq. (2)) and interaction with holes quickly trapped at OH sites (Eq. (3)) favour recombination.[26] Surface charge induced band banding leads to bottlenecks at nano-crystals interface.[27]

$$e_{free} + O_{2(g)} \rightarrow O^-_{2(ads)} \tag{2}$$

$$e_{(free)} + OH\cdot \rightarrow OH- \tag{3}$$

Once dry air is injected the background ambient is brought out of equilibrium with respect to TiO_2 surface. Photoconductivity enhancement at lower exposure (0.1 mbar of dry-air) seems

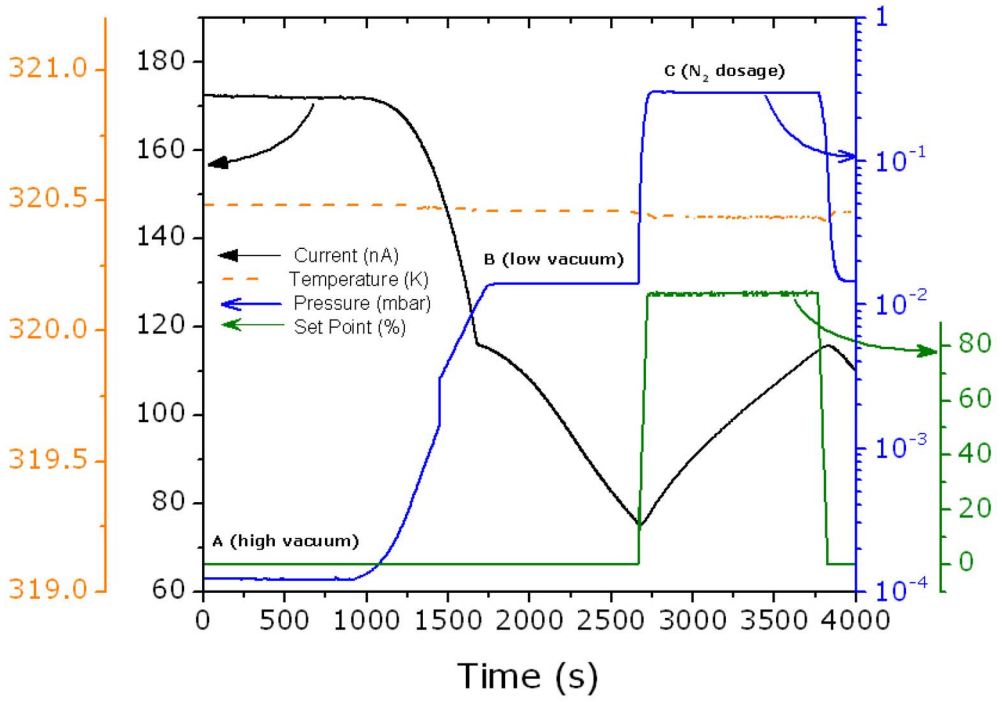

FIG. 7. Effect of the background ambient at a given pumping regime on photo-conductivity of TiO_2 mesoporous films (zones A and B). Effect of pure N_2 (zone C).

to indicate that the TiO_2 surface is partially depleted of recombination centers, the surface band banding is reduced or both.

To better understand this fact other experiments were performed. A sample was initially left to equilibrate with background ambient in vacuum at 10^{-4} mbar (see Fig. 7 for $t < 1000$ s). Then the turbo-molecular pump was stopped and the ambient conditions changed accordingly. At the same time the current dropped. This can be attributed to oxygen coming from the chamber leaks and pump back-stream. No other sources were present. Moreover as reported in Figure 7 at about 2600 s, nitrogen were dosed (0.2 mbar) and the current rose until N_2 was pumped out again.

Because nitrogen is expected to be inert on TiO_2 its effect on TiO_2 surface population should be different compared to oxygen's one. In our opinion the effect of nitrogen may be related to the dilution of the photo-adsorbed oxygen at surface with consequent reduction of oxygen-related effects on photo-conductivity. At the moment the same group is working on this effect on different prepared titania surface.

In summary it seems possible that different phenomena are responsible for similar photo-conductivity enhancement effects on illuminated TiO_2 mesoporous films. The important point within the context of this work is the possibility of clearly observing and repeatedly reproducing them by the present experimental set-up.

C. Reproducibility

As already pointed out, one crucial aspect of working with large surface area materials is the reproducibility of both sample preparation and characterization. In the following we present some data to better clarify the reliability of the present system about that. Series of samples were prepared and characterised in different moments, hence the starting conditions of both sample surface and vacuum chamber could be different in principle (pollutants on sample surface, ambient humidity). In this case support (a, b) hosts three nominally identical samples (A, B ,C), which were characterised in stable conditions after a common thermal treatment mandatory to remove most of

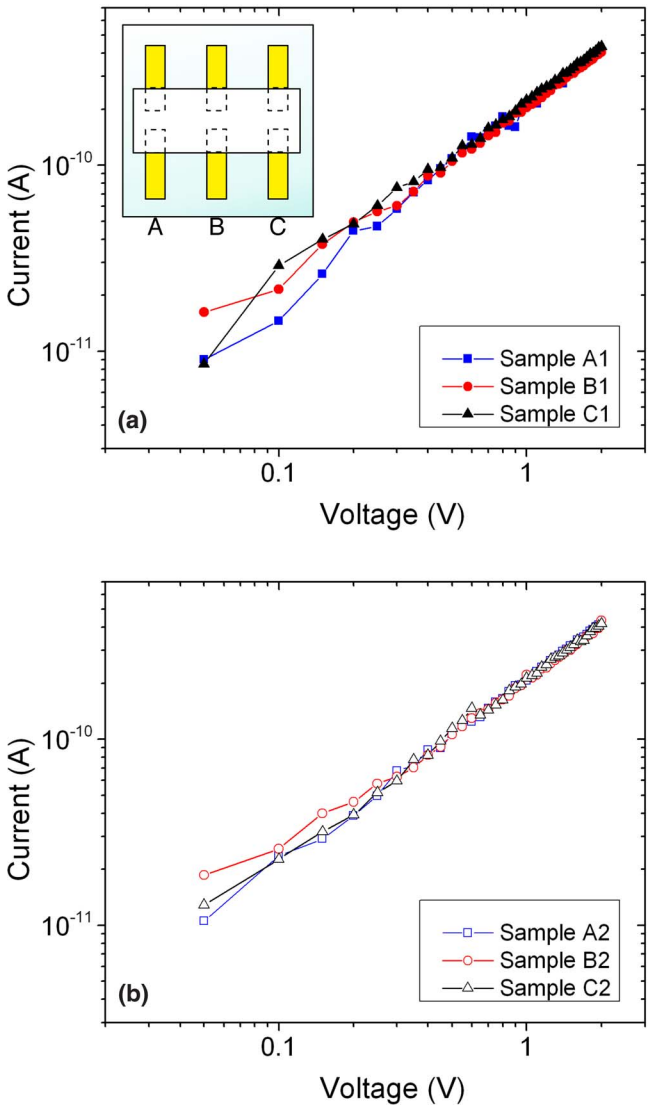

FIG. 8. Two sets of current-voltage characterization of anatase TiO_2 mesoporous films. The inset in "a" represents the contact geometry, inter-electrode distance was about 1 μm, sample to sample distance was 2 mm (not in scale); dashed lines show the electrode geometry under the printed titania. The two sets (a, b) were acquired in different experiments. Each curve (A, B, C) of the same run was taken during the same experiment.

the adsorbed water.[15] In Figure 8 are reported two sets of data from in dark electrical measurements on anatase thin films. The strong reproducibility between the sets of data confirms the similarity of the samples (a necessary but not sufficient condition), moreover shows that even for independent loading and preparation steps the system led likely to the same surface condition, and allowed for highly reproducible electrical characterization.

IV. CONCLUSIONS

We developed an integrated system for the electrical photo-characterization of sensing-oriented materials in strictly controlled experimental conditions. The reported experimental results show its capability of resolve the different effects of respectively adsorbed, condensed and bulk ethanol within the pore volume of free-standing meso-PS membranes. We remark that IR techniques, though selective and versatile for free carrier-related investigations, do not easily allow distinguishing these

different phenomena. Moreover typical gas dosage in spectroscopy starts from a few mbar, while this system allows for dosage of fractions of mbar. Our system also allows for discriminating competitive surface phenomena affecting TiO_2 porous films photo-conductivity by means of fine-tuned gas dosages and well-resolved current measurements.

ACKNOWLEDGMENTS

We would like to thank Prof. Elio Giamello (Dept. of Chemistry, University of Turin), Dr. Lorenzo Mino (Dept. of Chemistry, University of Turin) and Mr. Fabio Bertiglia (INRiM, Thermodynamics division) for many fruitful discussions. Mr. Roberto Rocci (INRiM, Nanofacility Piemonte) for the technical support. Carlo Lamberti thanks the support of "Progetti di Ricerca di Ateneo - Compagnia di San Paolo, 2011 - Linea 1", "ORTO11RRT5 project" and the "Mega-grant of the Russian Federation Government" to support scientific research under the supervision of leading scientist at Southern Federal University, No. 14.Y26.31.0001. This research has been partially funded by MIUR FIRB project "Thermalskin", grant RBFR10VZUG. *Nanofacility Piemonte* is a laboratory supported by Compagnia di San Paolo Foundation. "NaSERA" international programme contributed in funding for the experimental setup (Reinforcing Nanostructured material research cooperation between the Unit de Dveloppement de la Technologie du Silicium (UDTS) (now CRTSE) and the European Research Area (ERA), European Commission Directorate-General for Research and Innovation Grant Agreement No 295000).

[1] M. E. Davis, Nature **417**, 813–821 (2002).
[2] G. Korotcenkov and B. Cho, Critical Reviews in Solid State and Materials Sciences **35**, 153–260 (2010).
[3] J. M. Buriak, Philos. Trans. R. Soc. London Ser. A **364**, 217–225 (2006).
[4] M. Tiemann, Chemistry - A European Journal **13**, 8376–8388 (2007).
[5] C. Baratto, G. Faglia, G. Sberveglieri, Z. Gaburro, L. Pancheri, C. Oton, and L. Pavesi, Sensors **2**, 121–126 (2002).
[6] L. Pancheri, C. Oton, Z. Gaburro, G. Soncini, and L. Pavesi, Sensors and Actuators B: Chemical **89**, 237–239 (2003).
[7] E. Garrone *et al.*, Adv. Mater. **17**, 528–531 (2005).
[8] L. Boarino *et al.*, Mater. Sci. Eng. B **69**, 210–214 (2000).
[9] V. Y. Timoshenko, T. Dittrich, and F. Koch, Phys. Status Solidi B **222**, R1–R2 (2000).
[10] G. Amato *et al.*, J. App. Phys. **114**, 204302 (2013).
[11] M. A. Henderson, Surf. Sci. Rep. **66**, 185–297 (2011).
[12] L. Mino, G. Agostini, E. Borfecchia, D. Gianolio, A. Piovano, E. Gallo, and C. Lamberti, J. Phys. D: App. Phys. **46**, 423001 (2013).
[13] V. Galstyan, E. Comini, G. Faglia, A. Vomiero, L. Borghese, E. Bontempi, and G. Sberviglieri, Nanotechnology **23**, 235706 (2012).
[14] M. Gratzel, Inorg. Chem. **44**, 6841–6851 (2005).
[15] A. Cultrera, L. Boarino, G. Amato, and C. Lamberti, J. Phys. D: App. Phys. **47**, 015102 (2014).
[16] C. Faivre, D. Bellet, and G. Dolino, Eur. Phys. J. B **7**, 19–36 (1999).
[17] I. Schechter, M. Ben-Chorin, and A. Kux, J. Anal. Chem. **67**, 3727–3732 (1995).
[18] G. Gesele, J. Linsmeier, V. Drach, J. Fricke, and R. Arens-Fischer, J. Phys. D: App. Phys. **30**, 2911 (1997).
[19] V. Y. Timoshenko, T. Dittrich, V. Lysenko, M. G. Lisachenko, and F. Koch, Phys. Rev. B **64**, 085314 (2001).
[20] V. Lehmann, F. Hofmann, F. Möller, and U. Grüning, Thin Solid Films **255**, 20–22 (1995).
[21] D. Stroud, Superlattices and microstructures **23**, 567–573 (1998).
[22] B. Urbach, E. Axelrod, and A. Sa'ar, Phys. Rev. B **75**, 205330 (2007).
[23] I. Smallwood, *Handbook of Organic Solvent Properties* (Butterworth-Heinemann, 1996).
[24] S. A. Studenikin, N. Golego, and M. Cocivera, J. App. Phys. **84**, 5001–5004 (1998).
[25] N. Golego, S. Studenikin, and M. Cocivera, J. Electrochem. Soc. **147**, 1592–1594 (2000).
[26] G. Munuera, V. Rives-Arnau, and A. Saucedo, J. Chem. Soc. Faraday Trans. 1 **75**, 736–747 (1979).
[27] R. Van de Krol and H. Tuller, Solid State Ionics **150**, 167–179 (2002).